3D interconnected SnO2-coated Cu foam as a high-performance anode for lithium-ion battery applications

Article *in* RSC Advances · October 2014

DOI: 10.1039/C4RA12297F

RSC Advances

COMMUNICATION

View Article Online
View Journal | View Issue

Cite this: *RSC Adv.*, 2014, **4**, 58059

Received 13th October 2014
Accepted 30th October 2014

DOI: 10.1039/c4ra12297f

www.rsc.org/advances

3D interconnected SnO_2-coated Cu foam as a high-performance anode for lithium-ion battery applications†

Ji Hyun Um,[ab] Hyeji Park,[c] Yong-Hun Cho,*[c] Matthew P. B. Glazer,[d] David C. Dunand,[d] Heeman Choe[c] and Yung-Eun Sung*[ab]

A SnO_2-coated Cu foam with 3D interconnected scaffold was fabricated by a simple sol–gel method for use as a self-supporting anode for lithium-ion batteries. The binder- and carbon-free electrode integrated with a current collector exhibits a high reversible capacity, excellent rate capability, and stable cycle retention by preserving its structural integrity.

Tin dioxide (SnO_2) has been regarded as a promising alternative to the currently used graphite anode for next generation lithium-ion batteries (LIBs) because of its relatively low cost, low toxicity, high natural abundance, and, most importantly, low discharge potential and high theoretical capacity of 781 mA h g^{-1} from the maximum reaction to form $Li_{4.4}Sn$ alloy.[1–3] However, the large amounts of Li ions inserted/extracted into/from Sn induce severe volume changes (up to approximately 300%), which causes a pulverization of Sn particles and a loss of electrical contact with current collector, eventually resulting in poor electrochemical performance.[2–4]

Substantial efforts have been devoted to addressing this issue, and two approaches have been extensively investigated: a unique nanostructuring of SnO_2 for short Li ion diffusion paths and void spaces to accommodate the severe volume changes[4,5] and a nanocompositing with carbonaceous materials for enhanced electrical conductivity and structural stability resulted from the coating layer or matrix.[4,6] However, the introduction of carbonaceous materials into SnO_2 has an inherent weakness with respect to gravimetric specific capacity calculated from the combination of SnO_2 and carbon. Since the theoretical capacity of graphite, based on a reversible intercalation reaction, is 372 mA h g^{-1} (corresponding to LiC_6) which is considerably lower than that of SnO_2. Although in case of graphene the theoretical capacity is 740 mA h g^{-1} (corresponding to Li_2C_6) which is limited to the carbon composed predominantly of single layers.[7,8] Therefore, the unique morphology controls of SnO_2 using several synthetic methods have been proposed to achieve prolonged cycle stability without a decrease in the gravimetric specific capacity. Many researches for the morphology controls of SnO_2 have been accomplished, including one-dimensional (1D) nanorods,[9] nanotubes,[10] or nanowires;[11,12] two-dimensional (2D) nanosheets;[13,14] and three-dimensional (3D) nanoarchitectures.[15] Recently, the 3D scaffold architecture has attracted attention as a smart electrode prototype,[16,17] and various architectures from simple periodic arrays of cylindrical nanopillars[18] to complex arrangements such as inverse opal scaffold,[19] foams,[20,21] and long chains of particles[22,23] have been conducted.

In this work, we report a facile synthesis of SnO_2-coated Cu foam (SnO_2/Cu foam) as a self-supporting anode for LIBs. Through the use of a simple sol–gel method, a SnO_2/Cu foam integrated with current collector, and free of binder and conducting agent was obtained. A 3D interconnected metallic scaffold coated with high capacity material is advantageous for alleviating the large volume changes of active material and for the easy transport of electrons and Li ions.[4,15–17] The SnO_2/Cu foam exhibited a high reversible capacity of 621 mA h g^{-1} at a rate of 1 C after 50 cycles, an excellent rate capability of 368 mA h g^{-1} at 2 C, and a stable cycle performance, and its structural integrity was preserved after cycling.

The SnO_2/Cu foam was fabricated using a sol–gel method, and the synthesis process is shown in Fig. S1 (ESI†). The procedure for synthesizing the electrode is described in more detail in ESI.† Fig. 1 shows the surface morphology of commercially available Cu foam in the pristine state (Fig. 1a–c) and after SnO_2 sol–gel coating (Fig. 1d–f). In Fig. 1a, prior to coating with SnO_2, the Cu foam was a 3D interconnected

[a]*School of Chemical & Biological Engineering, Seoul National University, Seoul 151-742, Republic of Korea*

[b]*Center for Nanoparticle Research, Institute for Basic Science (IBS), Seoul 151-742, Republic of Korea. E-mail: ysung@snu.ac.kr*

[c]*School of Advanced Materials Engineering, Kookmin University, Seoul 136-702, Republic of Korea. E-mail: yhun00@kookmin.ac.kr*

[d]*Department of Materials Science and Engineering, Northwestern University, Evanston, IL 60208, USA*

† Electronic supplementary information (ESI) available. See DOI: 10.1039/c4ra12297f

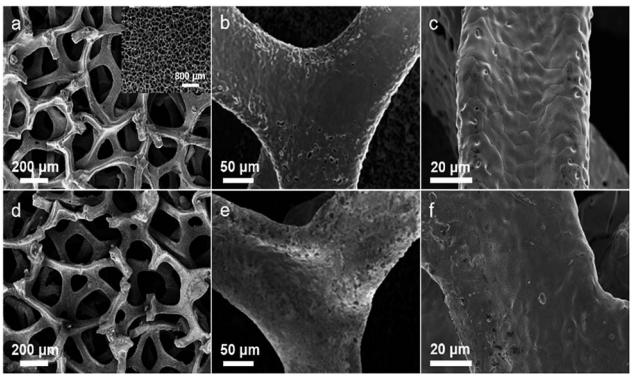

Fig. 1 FE-SEM images of Cu foam at pristine state (a)–(c) and after SnO_2 sol–gel coating (d)–(f). The inset shows the pristine Cu foam at low magnification.

scaffold composed of continuous struts with a width of less than approximately 100 μm and of interconnected pores with a diameter of 100–500 μm. This morphology character is also confirmed at lower magnification in the inset of Fig. 1a. The surface of the struts was further examined using higher magnification FE-SEM images (Fig. 1b and c), and the development of small pores and grains on the surface was observed. After SnO_2 coating, the 3D interconnected scaffold of the Cu foam was maintained as shown in Fig. 1d, and the surface morphology of the Cu foam was relatively smooth with covering the small pores and the grains (Fig. 1e and f). Fig. 2a–d present FE-SEM and EDX mapping images of the Cu foam after SnO_2 coating. The presence of Cu, Sn, and O was confirmed, and the distributions of Sn and O corresponded with that of Cu, which implies that the Cu foam served as a template for the deposition of SnO_2. To confirm the thickness of the SnO_2 deposited as a coating layer, the cross-sectional image of Fig. 2a obtained using FIB milling is presented in Fig. 2e. The inset shows a whole cross-sectional image of the SnO_2/Cu foam, and the magnified image indicates that the Cu foam was covered with a thin (approximately 200 nm) and uniform layer. This coating layer is presumed to be SnO_2 based on the EDX mapping (Fig. S2a, ESI†), and its thickness of approximately 200 nm was confirmed from the EDX line scan (Fig. S2b, ESI†). The XRD pattern in Fig. S3 (ESI†) confirms the presence of the SnO_2

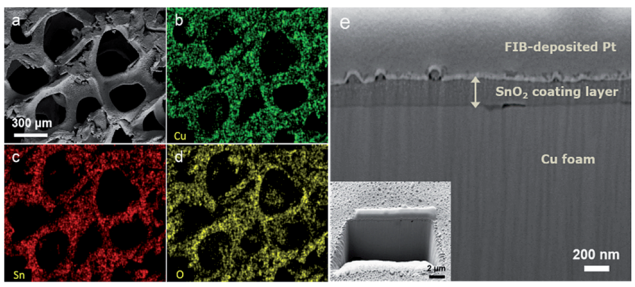

Fig. 2 FE-SEM images of SnO_2-coated Cu foam using EDX mapping (a)–(d) and using FIB milling (e). The inset shows the cross-sectional SnO_2-coated Cu foam at low magnification.

because only peaks for tetragonal rutile SnO_2 (JCPDS 41-1445) and metallic Cu (JCPDS 04-0836) are observed with no additional peaks such as SnO and Cu_2O.[24–26]

The SnO_2 sol–gel concentration was initially investigated under the assumption that the Sn(II) molar concentration may or may not have an impact on the electrochemical performance. SnO_2/Cu foams were prepared from different Sn(II) molar concentrations of 3 M and 10 M, and these foams were referred to as SnO_2/Cu foam@3M and SnO_2/Cu foam@10M, respectively. To understand the reactive processes of the SnO_2/Cu foam@3M and SnO_2/Cu foam@10M, cyclic voltammetry (CV) measurement was conducted in the voltage range of 0.01–2 V at a scan rate of 0.1 mV s^{-1} (Fig. S4, ESI†). The first five CV curves of SnO_2/Cu foam@3M and SnO_2/Cu foam@10M were in accord with the electrochemical behaviour of SnO_2-based materials.[27–29] The first cathodic peak at 0.64 V of the SnO_2/Cu foam@3M is ascribed to the irreversible formation of a solid electrolyte interface (SEI) layer due to electrolyte decomposition and the reduction of SnO_2 to Sn as followed by eqn (1) and (2), respectively.

$$Li^+ + e^- + \text{electrolyte} \rightarrow \text{SEI (Li)} \quad (1)$$

$$SnO_2 + 4Li^+ + 4e^- \rightarrow Sn + 2Li_2O \quad (2)$$

$$Sn + xLi^+ + xe^- \rightarrow Li_xSn\ (0 \leq x \leq 4.4) \quad (3)$$

In addition, the cathodic peaks at 0.0–0.5 V indicate the formation of Li_xSn alloys as described by eqn (3), and the corresponding anodic peaks appeared at 0.2–1.0 V because of the extraction of Li ions from the Li_xSn alloys.[30] The anodic peak appeared at 1.42 V, which is attributed to the oxidation of Sn to SnO_2, and the first cathodic peak shifted to higher voltages by around 0.94 V during subsequent cycles, which implies partial reversibility of the electrochemical reaction described by eqn (2).[29,31] A battery performance test was carried out to examine the potential of SnO_2/Cu foam@3M and SnO_2/Cu foam@10M as anode for LIBs. Fig. S5a (ESI†) presents the first two voltage profiles of SnO_2/Cu foam@3M and SnO_2/Cu foam@10M in the voltage range of 0.01–2 V at a current density of 1 C (1 C = 781 mA g^{-1}), and these voltage profiles are consistent with the corresponding CV curves (Fig. S4, ESI†) and with the lithiation/delithiation process described in previous reports.[22,31] The cycling performances of SnO_2/Cu foam@3M and SnO_2/Cu foam@10M at 1 C are shown in Fig. S5b (ESI†). Both electrodes exhibited stable capacity retention, and the capacity of SnO_2/Cu foam@10M was approximately 200 mA h g^{-1} higher than that of SnO_2/Cu foam@3M throughout all of the cycles. Although the reason for the increase in capacity with increasing Sn(II) molar concentration is not yet clear, the 10 M Sn(II) solution was used in our investigation of high capacity electrode.

The electrochemical properties of the SnO_2/Cu foam were further examined by introducing a commercial SnO_2 powder electrode which was pasted on a Cu foil and referred to as SnO_2 NPs, as a control group. The cycling performances of the SnO_2/Cu foam and SnO_2 NPs at 1 C between 0.01 and 2 V are presented in Fig. 3a. Although the capacities of both SnO_2/Cu foam

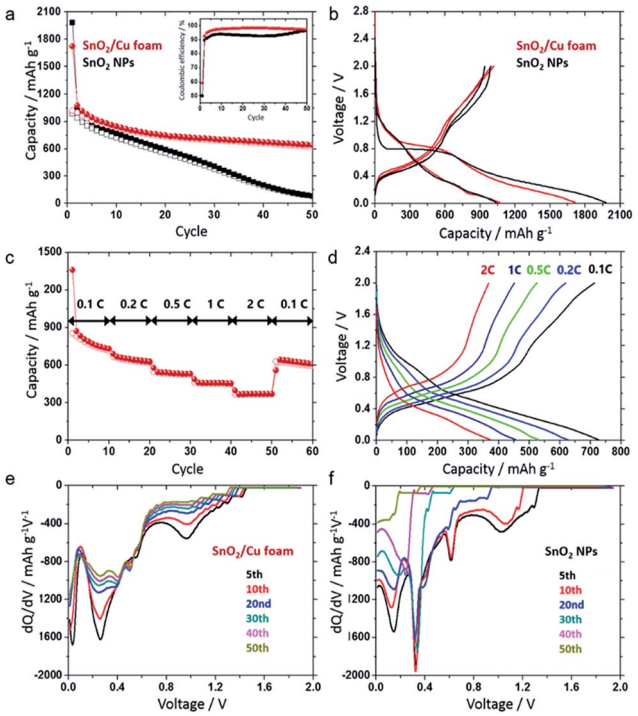

Fig. 3 (a) Cycle performance of SnO_2/Cu foam and SnO_2 NPs at 1 C for 50 cycles with the inset of coulombic efficiencies, (b) voltage profiles of SnO_2/Cu foam and SnO_2 NPs during the first two cycles at 1 C, (c) capacity and (d) voltage profiles of SnO_2/Cu foam cycled at various rates, and (e) dQ/dV profiles of SnO_2/Cu foam and (f) of SnO_2 NPs at 1 C at selected cycle.

and SnO_2 NPs decreased in the early cycles, the SnO_2/Cu foam subsequently exhibited stable capacity retention and a reversible capacity as high as 621 mA h g^{-1} after 50 discharge/charge cycles. The high Li ion storage of the SnO_2/Cu foam is fairly comparable to that of recently reported Sn-based anode materials (see the comparison in Table S1, ESI†). Additionally, the coulombic efficiencies of the SnO_2/Cu foam (inset of Fig. 3a) remained relatively stable, whereas those of the SnO_2 NPs were considerably lower and fairly unstable over all of the cycles. The commercially available Cu foam with 500 μm thickness was directly employed to an electrode. The thickness of Cu foam was thicker than the conventional Cu foil with 20 μm and also the previous 3D scaffold electrode with 160 μm,[32] 59 μm,[33] and 10 μm.[19] The large difference of the electrode thickness in magnitude can be reduced by introducing a physically cutting or polishing step and a compression process under high pressure.[32,33] The possibility to increase the volumetric energy density by reducing the thickness of Cu foam exists in our work. As shown in Fig. 3b, the first discharge and charge capacities of the SnO_2/Cu foam were 1720 and 1017 mA h g^{-1}, respectively, and those of the SnO_2 NPs were 1983 and 988 mA h g^{-1}, respectively, which indicates that the coulombic efficiency of the SnO_2/Cu foam was 10% higher than that of the SnO_2 NPs. Additionally, the second charge capacities of the SnO_2/Cu foam and SnO_2 NPs were 998 and 938 mA h g^{-1}, respectively. From a comparison of the first and second charge capacities, the rate of decrease in the capacity of the SnO_2 NPs is approximately 2.7 times faster than that of the SnO_2/Cu foam. The rate capability of the SnO_2/Cu foam cycled between 0.01 and 2 V was evaluated stepwise by increasing the C-rate from 0.1 C to 2 C and then returning to 0.1 C as shown in Fig. 3c. When cycled at 0.1 C, the first charge capacity of 852 mA h g^{-1} decreased to 713 mA h g^{-1} for the subsequent 10 cycles, and then the capacity became stable as the C-rate increased. At a significantly high rate of 2 C (1562 mA g^{-1}), the SnO_2/Cu foam delivered a high capacity of 368 mA h g^{-1} with good stability, which is comparable with recent reports on Sn-based materials,[34,35] or even better.[36–38] When the C-rate was reduced back to 0.1 C after 50 cycles, the SnO_2/Cu foam recovered a respectable amount of the first 0.1 C step capacity, demonstrating its excellent rate capability. Fig. 3d presents the last discharge/charge voltage profiles of each rate step shown in Fig. 3c. As the C-rate increased, the lithiation potential decreased and the delithiation potential increased, which is due to the kinetic effects of the material.[39] Moreover, the lithiation potential at a significantly high rate of 2 C exhibited a sloping profile between 0.01 and 0.3 V, corresponding to the formation of Li_xSn alloy.[27–29,40] The differential capacity profiles (dQ/dV *vs.* voltage) of the SnO_2/Cu foam and SnO_2 NPs are shown in Fig. 3e and f. The distinct peaks between 0.0 and 0.7 V correspond to the lithiation steps for forming the Li_xSn alloys. For the SnO_2/Cu foam, the intensities corresponding to the Li_xSn peaks diminished with a slowly decreasing rate, and they retained a relatively large area after 50 cycles. This feature is also observed in the SnO_2/Cu foam prepared from a sol–gel concentration of 3 M (Fig. S6, ESI†). However, the intensities of the SnO_2 NPs rapidly decreased and nearly disappeared at the 50th cycle, which suggests that the insertion of Li ions into the SnO_2 NPs no longer occurs, which is in contrast to the SnO_2/Cu foam. The clearly stable Li ion storage of the SnO_2/Cu foam may be attributed to its 3D interconnected structure, effectively accommodating the large volume changes of Sn with repeated lithiation/delithiation processes, and thereby preventing the pulverization of Sn particles and the loss of its electrical connection.

To certify the stabilizing effect of the SnO_2/Cu foam, the cells of both SnO_2/Cu foam and SnO_2 NPs after 50 cycles at 1 C were disassembled and examined as shown in Fig. S7 (ESI†). The electrode morphology of the SnO_2/Cu foam retained its original architecture after cycling, whereas that of the SnO_2 NPs was quite different. In contrast to the SnO_2/Cu foam, the poor contact between SnO_2 nanoparticles and current collector in the SnO_2 NPs resulted in the rapid capacity fading. To further examine the surface and cross-sectional morphology of the SnO_2/Cu foam, the electrode after cycling was investigated using FE-SEM and FIB milling. As shown in Fig. 4a, the morphology of the SnO_2/Cu foam after cycling was similar to that before cycling (Fig. 1d). Moreover, the SnO_2 coating layer on the Cu foam was still present after 50 cycles, and its thickness increased to 480 nm, corresponding to an expansion ratio of ~153% based on a comparison of the SnO_2 thickness before (Fig. 4b) and after (Fig. 4c) cycling. The presence of the stable SnO_2 coating layer on the Cu foam without severe separation from current collector maintained the electrical connection to

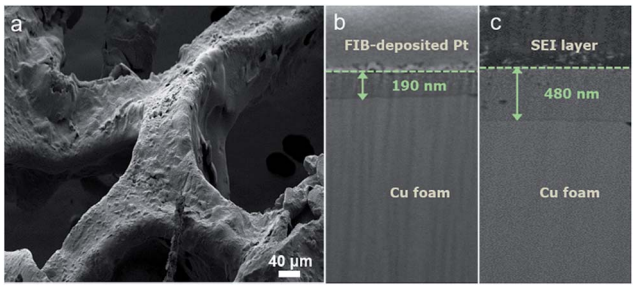

Fig. 4 (a) FE-SEM image of SnO_2/Cu foam after 50 cycles and (b) and (c) cross-sectional image of SnO_2/Cu foam before and after cycling, respectively.

the Cu foam, which provided the electrode with excellent cycling performance. As a further check for the stability of the anode, In operando X-ray diffraction was also performed on the SnO_2/Cu foam at 1 C (Fig. S8, ESI†), to monitor the evolution of strain in the Cu foam in response to (de)lithiation of the Sn during cycling. The elastic strain behaviour in Fig. S8† indicates that (de)lithiation-induced mismatch strains are created by load transfer from the expanding/contracting SnO_2 coating layer to the Cu foam, and increase/decrease (i) linearly with respect the extent of (de)lithiation (and thus the amount of mismatch), (ii) reversibly during a full lithiation/delithiation cycle, and (iii) with good repeatability over 20 cycles. This is consistent with the Cu foam scaffold acting as a partial mechanical constraint for the lithiation of the SnO_2 coating layer, as observed also recently in an inverse-opal Ni scaffold coated with Si.[41] However, the Cu strains are low and within the elastic strain region for Cu, suggesting that the much larger mismatch due to (de)lithiation is mostly accommodated by expansion into the pores. The high repeatability between the various cycles in Fig. S9† indicates good mechanical (and thus also electrical) contact between the SnO_2 coating layer and the Cu foam current collector.

Conclusions

In summary, a SnO_2-coated Cu foam was obtained through a simple sol–gel synthesis, and was electrochemically investigated as an anode for LIBs. This electrode, which was integrated with current collector and without the addition of binder and conducting agent, delivered a high reversible capacity of 621 mA h g^{-1} at 1 C after 50 cycles and an excellent rate performance of 368 mA h g^{-1} at 2 C. The high Li ion storage and rate capability were attributed to the 3D continuous Cu foam scaffold and the interconnected porous structure for the facile transport of electrons and Li ions. From a comparison with the conventional SnO_2 nanoparticle electrode, the superiority of 3D scaffold architecture, particularly for the alleviating the severe volume changes of Sn, was demonstrated by preserving its original architecture. These results indicate that the SnO_2/Cu foam has promising applications as a self-supporting, binder- and carbon-free anode for advanced LIBs.

Acknowledgements

Y.-E. S. acknowledges the Institute for Basic Science (IBS) in Korea. This work was supported by Project Code (IBS-R006-G1). Y. H. C. acknowledges financial support from the Priority Research Center Program (2009-0093814) and the Basic Science Research Program (2013R1A1A2061636) through the National Research Foundation of Korea (NRF), which is funded by the Ministry of Education. H. C. also acknowledges financial support from the Pioneer (2011- 0001684) Program through NRF of Korea. M. P. B. G. acknowledges G. Halder (Advanced Photon Source) for assistance with in operando XRD data collection. This research used resources of the Advanced Photon Source, a U.S. Department of Energy (DOE) Office of Science User Facility operated for the DOE Office of Science by Argonne National Laboratory under Contract no. DE-AC02-06CH11357.

Notes and references

1 Y. Idota, T. Kubota, A. Matsufuji, Y. Maekawa and T. Miyasaka, *Science*, 1997, **276**, 1395.
2 I. A. Courtney and J. R. Dahn, *J. Electrochem. Soc.*, 1997, **144**, 2045.
3 T. Brousse, R. Retoux, U. Herterich and D. M. Schleich, *J. Electrochem. Soc.*, 1998, **145**, 1.
4 J. S. Chen and X. W. Lou, *Small*, 2013, **9**, 1877.
5 Z. Wang, L. Zhou and X. W. Lou, *Adv. Mater.*, 2012, **24**, 1903.
6 G. Cui, Y.-S. Hu, L. Zhi, D. Wu, I. Lieberwirth, J. Maier and K. Müllen, *Small*, 2007, **3**, 2066.
7 J. R. Dahn, T. Zheng, Y. Liu and J. S. Xue, *Science*, 1995, **270**, 590.
8 R. Mukherjee, A. V. Thomas, A. Krishnamurthy and N. Koratkar, *ACS Nano*, 2012, **6**, 7867.
9 J. Liu, Y. Li, X. Huang, R. Ding, Y. Hu, J. Jiang and L. Liao, *J. Mater. Chem.*, 2009, **19**, 1859.
10 J. Ye, H. Zhang, R. Yang, X. Li and L. Qi, *Small*, 2010, **6**, 296.
11 M.-S. Park, G.-X. Wang, Y.-M. Kang, D. Wexler, S.-X. Dou and H.-K. Liu, *Angew. Chem., Int. Ed.*, 2007, **46**, 750.
12 J. Y. Huang, L. Zhong, C. M. Wang, J. P. Sullivan, W. Xu, L. Q. Zhang, S. X. Mao, N. S. Hudak, X. H. Liu, A. Subramanian, H. Fan, L. Qi, A. Kushima and J. Li, *Science*, 2010, **330**, 1515.
13 S. Ding, J. S. Chen and X. W. Lou, *Adv. Funct. Mater.*, 2011, **21**, 4120.
14 H. B. Wu, J. S. Chen, X. W. Lou and H. H. Hng, *J. Phys. Chem. C*, 2011, **115**, 24605.
15 X. Li, A. Dhanabalan, L. Gu and C. Wang, *Adv. Energy Mater.*, 2012, **2**, 238.
16 H. Zhang, X. Yu and P. V. Braun, *Nat. Nanotechnol.*, 2011, **6**, 277.
17 X. Zhu, Z. Guo, P. Zhang, G. Du, R. Zeng, Z. Chen and H. Liu, *ChemPhysChem*, 2009, **10**, 3101.
18 L. Ji, Z. Tan, T. Kuykendall, E. J. An, Y. Fu, V. Battaglia and Y. Zhang, *Energy Environ. Sci.*, 2011, **4**, 3611.
19 H. Zhang and P. V. Braun, *Nano Lett.*, 2012, **12**, 2778.

20 Y. Fu, Z. Yang, X. Li, X. Wang, D. Liu, D. Hu, L. Qiao and D. He, *J. Mater. Chem. A*, 2013, **1**, 10002.
21 W. Ni, H. B. Wu, B. Wang, R. Xu and X. W. Lou, *Small*, 2012, **8**, 3432.
22 J. Lin, Z. Peng, C. Xiang, G. Ruan, Z. Yan, D. Natelson and J. M. Tour, *ACS Nano*, 2013, **7**, 6001.
23 Y. Yu, L. Gu, C. Wang, A. Dhanabalan, P. A. van Aken and J. Maier, *Angew. Chem., Int. Ed.*, 2009, **48**, 6485.
24 J. Y. Xiang, J. P. Tu, Y. F. Yuan, X. H. Huang, Y. Zhou and L. Zhang, *Electrochem. Commun.*, 2009, **11**, 262.
25 M. Bhagwat, P. Shah and V. Ramaswamy, *Mater. Lett.*, 2003, **57**, 1604.
26 Y.-Y. Zhu, S.-R. Wang, L.-J. Zhu, X.-L. Ge, X.-B. Li and Z.-Y. Luo, *Catal. Lett.*, 2010, **135**, 275.
27 J. Li, Y. Zhao, N. Wang and L. Guan, *Chem. Commun.*, 2011, **47**, 5238.
28 Y. Zhao, J. Li, N. Wang, C. Wu, G. Dong and L. Guan, *J. Phys. Chem. C*, 2012, **116**, 18612.
29 Y. Yang, X. Ji, F. Lu, Q. Chena and C. E. Banks, *Phys. Chem. Chem. Phys.*, 2013, **15**, 15098.
30 K. Kravchyk, L. Protesescu, M. I. Bodnarchuk, F. Krumeich, M. Yarema, M. Walter, C. Guntlin and M. V. Kovalenko, *J. Am. Chem. Soc.*, 2013, **135**, 4199.
31 R. Demir-Cakan, Y.-S. Hu, M. Antonietti, J. Maier and M.-M. Titirici, *Chem. Mater.*, 2008, **20**, 1227.
32 H. Ji, L. Zhang, M. T. Pettes, H. Li, S. Chen, L. Shi, R. Piner and R. S. Ruoff, *Nano Lett.*, 2012, **12**, 2446.
33 J. Ji, H. Ji, L. L. Zhang, X. Zhao, X. Bai, X. Fan, F. Zhang and R. S. Ruoff, *Adv. Mater.*, 2013, **25**, 4673.
34 D. Wang, X. Li, J. Yang, J. Wang, D. Geng, R. Li, M. Cai, T.-K. Sham and X. Sun, *Phys. Chem. Chem. Phys.*, 2013, **15**, 3535.
35 B. Luo, B. Wang, M. Liang, J. Ning, X. Li and L. Zhi, *Adv. Mater.*, 2012, **24**, 1405.
36 H. Zhang, H. Song, X. Chen and J. Zhou, *J. Phys. Chem. C*, 2012, **116**, 22774.
37 C. Wang, Y. Li, Y.-S. Chui, Q. H. Wu, X. Chen and W. Zhang, *Nanoscale*, 2013, **5**, 10599.
38 B. Luo, B. Wang, X. Li, Y. Jia, M. Liang and L. Zhi, *Adv. Mater.*, 2012, **24**, 3538.
39 H. W. Lee, P. Muralidharan, R. Ruffo, C. M. Mari, Y. Cui and D. K. Kim, *Nano Lett.*, 2010, **10**, 3852.
40 H. Wu, G. Yu, L. Pan, N. Liu, M. T. McDowell, Z. Bao and Y. Cui, *Nat. Commun.*, 2014, **4**, 1943.
41 D. C. Dunand, Presented in part at 2014 TMS Annual Meeting & Exhibition, San Diego, February 2014.